Multi-scale simulation framework for the modelling of charge capture and emission in spin qubit devices

G. Boschetto[1†], C. Wilhelmer[2†], L. Cvitkovich[3†], J. Li[1], D. Waldhoer[2], T. Grasser[2] and B. Martinez[1*]
[1]Univ. Grenoble Alpes, CEA, Leti, F-38000, Grenoble, France. *email: biel.martinezidiaz@cea.fr
[2]Institute for Microelectronics, TU Wien, Vienna, 1040, Austria
[3]Institute for Theoretical Physics, University of Regensburg, 93040 Regensburg, Germany
[†]These authors contributed equally to this work.

***Abstract*—** Charge transfer events can degrade the performance of spin qubits by inducing instabilities and decoherence. We present a multi-scale simulation approach to model these transitions and quantify their impact on qubit properties. Applying this framework to hole transfer between hydrogen bridge defects in SiO_2 and nearby gates, we find that, while their slow dynamics and large electrostatic impact rule them out as the main source of charge-noise-driven decoherence, such events can account for observed device instabilities.

I. Introduction

The spin of electrons and holes in Si MOS devices is a promising candidate for quantum computation due to the small size of the computational unit cell and its compatibility with standard microelectronics fabrication processes [1]–[3]. Reliable qubit operation, however, requires stable and uniform electrical environments. Differences in the electrostatic potentials can cause qubit-to-qubit variability [4], whereas temporal fluctuations—known as charge noise—degrade stability and spin coherence [5]. Despite its importance, the atomistic origin of charge noise remains unknown.

In Si MOS devices, the native amorphous oxide SiO_2 inevitably hosts atomic defects capable of trapping and exchanging charges with nearby gates [6]. When charged, these defects are known to be a source of static qubit-to-qubit variability [4]. If charge transitions occur on timescales shorter than the experiment (usually below 10^2 s), they could also dynamically impact the qubit properties. We can differentiate between different types of effects depending on the timescale of the charge transfers. If they only occur up to a few times during the experiment, they may be responsible for device instabilities, which can manifest as sudden shifts of the qubit properties. If the dynamics are very fast with respect to the experimental timescale, these events would appear as high frequency electric noise, known as charge noise, and drive spin decoherence.

Here, we present a multi-scale simulation framework to investigate charge transfer at cryogenic temperatures. The proposed methodology links the atomistic structure of the defects and their impact on the spin qubit properties. In Sec. **II** we describe in detail the simulation methodology, and in Sec. **III** we illustrate its application to hydrogen bridge (HB) defects in SiO_2. We finally conclude in Sec. **IV**.

II. Methodology

The simulation workflow combines atomistic and device-scale simulations. We use density functional theory (DFT) to model charged and neutral defect configurations by employing the CP2K code and the PBE0 hybrid functional. The amorphous sample structure was created by simulating a melt-and-quench procedure on cristobalite with molecular dynamics. We extract the configuration coordinate change ΔQ, the relaxation energy E_{R} and the energy difference between neutral and positive states ΔE from the geometry optimized defect configurations in charge states 0 and $+1$. ΔE is evaluated from the thermodynamic charge-state transition level (CTL) to study hole transfer between the gate and the defect site ($E_F = 5.11$ eV above the SiO_2 valence band maximum (VBM) [8]). The full computational details are given in Ref. [7] and the 1D configuration coordinate diagram constructed from these properties is sketched in Fig. 1.

We then apply nonradiative multiphonon (NMP) theory [7], [9]–[11] to extract the line shape functions (ξ) and compute the cryogenic charge transfer rates (k). In particular, we make use of the full Quantum Mechanical expression of the Nonradiative Multi-Phonon (NMP) model. The calculation of ξ takes the above-mentioned DFT data as input parameters ($\xi = f(\Delta Q, E_R, \Delta E, T)$, see Ref. [7] for the full derivation and expressions). k can then be then computed as

$$k = \sqrt{n\Omega}\frac{2\pi|V_{\mathrm{c}}|^2}{\hbar}\xi, \tag{1}$$

with $\sqrt{n\Omega}$ quantifying the available number of states in the charge reservoir. n is the density of states near the Fermi energy of the metal (here we take $n = 10^{19}\,\mathrm{cm}^{-3}$ [8]), and Ω is the volume of the charge reservoir in the simulation cell of the prefactor extraction simulation ($2.17 \cdot 10^{-21}\,\mathrm{cm}^3$ in Ref. [12]). V_{C} is the electronic coupling matrix element between the initial and final charge state. Its expression can be approximated within WKB to an exponential decay on the defect–gate distance as shown in Ref. [12],

$$V_{\mathrm{c}} = V_{\mathrm{c}}^0 \exp\left(-\sqrt{\frac{2m_t V}{\hbar}}\, d\right), \tag{2}$$

where $m_t = 0.33m_0$ is the hole effective mass in thin SiO_2 films [13], V is the energy barrier that the hole must

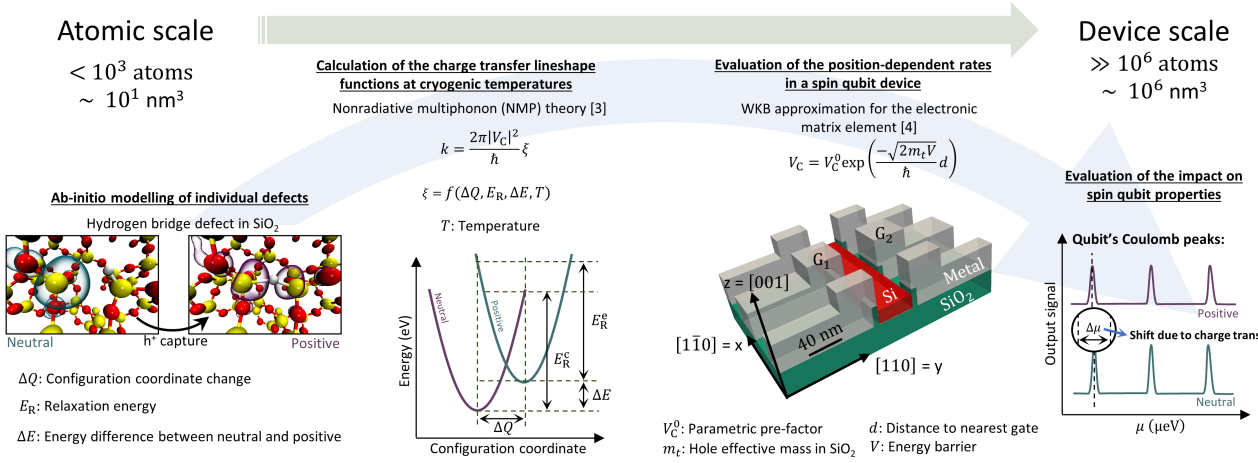

Fig. 1. Schematic representation of the multi-scale simulation workflow. DFT simulations are used to extract the defect properties (ΔQ, E_R, ΔE) at the atomistic level. The inset atomic structure shows an example of HB with the isosurface of the highest occupied molecular orbital of the neutral defect, and the lowest unoccupied molecular orbital of the charged defect. The defect parameters are then used to compute the line shape functions and charge transfer rates at cryogenic temperatures with a Wentzel–Kramers–Brillouin (WKB) approximation of the Nonradiative Multi-Phonon (NMP) model, and accounting for the specific position of the defect in the device. The complete expressions for ξ are fully developed and can be found in Refs. [7]. Finally, the impact of these events on the properties of spin qubits is evaluated by performing 3D numerical simulations at the device level using a $k \cdot p$ method [4]. As an illustration, the studied property is the shift of the qubit's coulomb peak ($\Delta\mu$) induced by a charge transfer event between the defect and a metallic gate.

overcome to trigger the charge transition, d is the distance to the nearest gate, and V_c^0 is a parametric prefactor that scales the exponential decay. We fix $V_\mathrm{c}^0 = 0.046\,\mathrm{eV}$ based on DFT estimates in similar systems [12].

The impact of the capture/emission events on spin qubit properties is evaluated through 3D device simulations. We solve Poisson's equation, and we feed the electrostatics to the six-band $k \cdot p$ Hamiltonian that we numerically solve with finite differences in the device mesh [14]. We can then extract measurable charge and spin quantities of the spin qubits. We hereafter focus on the first coulomb peak on the charge stability diagram, which is simply the ground-state energy of the qubit. We evaluate the shift induced by the charge transition to the coulomb peak by simulating the position of the coulomb peak for the neutral (μ_0) and positively charged (μ_+) defect and taking the difference,

$$\Delta\mu = \mu_+ - \mu_0. \tag{3}$$

This multi-scale simulation approach directly links measurable qubit shifts to the atomistic nature and position of defects, and may enable the identification of the nature and origin of the limiting defects.

III. Results

In this section, we apply the methodology described above to study charge transfer events between metallic gates and HB defects in SiO_2 within a hole Si MOS spin qubit device. We performed DFT simulations on 46 independent configurations of HB defects in amorphous SiO_2. In Fig. 2a we provide the obtained DFT results. The HB defects show large ΔQ, fingerprint of strong atomic reorganization when undergoing a charge transfer event. The relaxation energies are consequently also significant, averaging more than 2 eV. Interestingly, ΔE is systematically negative, which suggests that HB defects are preferably in the neutral charge state in the thermodynamic equilibrium.

We then computed the corresponding line shape functions at $T = 1\,\mathrm{K}$ the for capture and emission events. Note that, as shown in Eq. 1, the magnitude of ξ defines the rate up to a multiplicative factor. The line shape functions for emission are notably larger than those for capture events, owing to the negative ΔE. Indeed, with neutral states being energetically favorable, emissions are more likely to occur. Next, we evaluated the dependence of k on the physical distance (d) between the initial and final position of the charge. The distance dependence appears in the exponential part of the electronic matrix element of Eq. 1, and the exponential decay is also ruled by the energy barrier V. For the capture event, the hole is transferred from the gate Fermi level (E_F) to the trap level through the valence band, so $V = 5.11\,\mathrm{eV}$ for all defects (see Fig. 2b). Hole emissions involve the inverse process, so V is defect-dependent and it is ruled by ΔE.

In Fig. 3a we show the cryogenic capture and emission rates for a representative gate-defect distance $d = 0.5\,\mathrm{nm}$. Note that this is already a very small distance given the nature of the studied defect. Indeed, HB defects involve two Si atoms, and may therefore be more likely to be found a bit further from the gates. Still, for $d = 0.5\,\mathrm{nm}$ results already highlight very slow dynamics, with only a few defects being active within the experimental timescale.

Additionally, in Fig. 3b we show the ratio (in log scale) between the capture and emission rates for each individual defect. Indeed, we recovered the same trend observed for the line shape functions, with k_e being systematically larger than

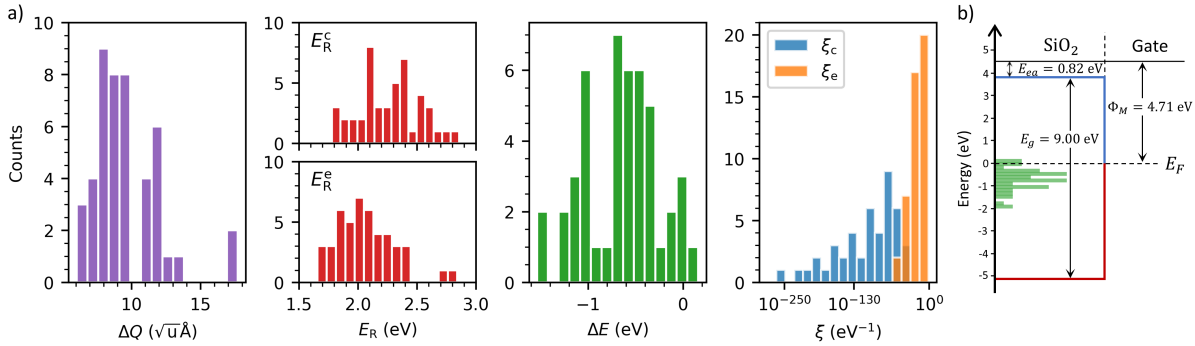

Fig. 2. a) Distribution of configuration coordinate change (ΔQ), relaxation energies for capture and emission ($E_{\mathrm{R}}^{\mathrm{c}}$, $E_{\mathrm{R}}^{\mathrm{e}}$), thermodynamic trap levels ΔE for hole transfer with the gate, and line shape functions for the capture (ξ_{c}) and emission (ξ_{e}) process at $T = 1\,\mathrm{K}$ for the 46 studied individual HB defects. The line shape functions have been computed by using the DFT data listed here and using the analytical expression of the WKB approximation for the NMP theory fully developed in Ref. [7]. b) Schematic representation of the SiO_2/gate band structure, with the trap levels of the 46 studied defects in green. The valence band of the SiO_2 is shown in red, and the conduction band in blue. The Fermi level (E_F) is placed at the metal work function (Φ_M).

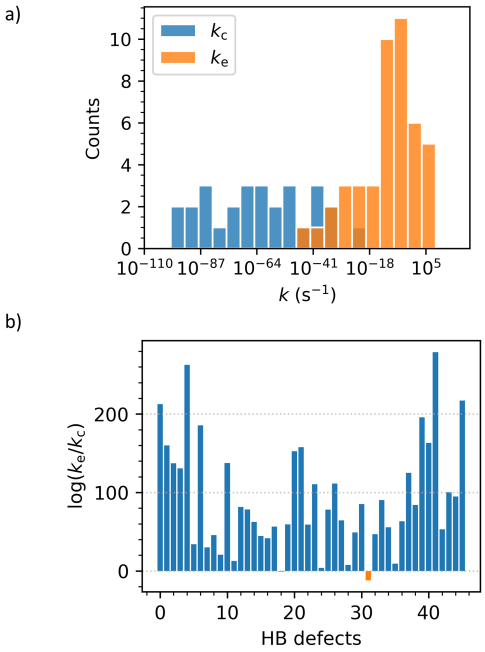

Fig. 3. a) Histogram of the capture (k_{c}) and emission (k_{e}) rates for all 46 simulated defects at a distance $d = 0.5\,\mathrm{nm}$ from the nearest gate. 18 defects with $k_{\mathrm{c}} < 10^{-110}\,\mathrm{s}^{-1}$ are not shown for clarity. b) Ratio (in log scale) between the emission and capture rates for all simulated HB defects.

k_{c}. In fact, only 2 defects out of the 46 display capture faster than emissions. Consequently, HB defects may experience eventual hole emissions but they are very unlikely to undergo subsequent hole trapping. This suggests that their charge transfer events are unlikely to provide random telegraph signals but rather sparse switches due to isolated emission events.

We next evaluated the dependence of k on the actual position of the defect in the realistic spin qubit device shown in Fig. 2. Note that the charge transfer takes place between the defect and the metallic gates of the device. We chose as an illustration a HB defect with $\xi_{\mathrm{e}} = 1.44{\cdot}10^{-1}\,\mathrm{eV}^{-1}$ (the largest in Fig. 2a), and we sampled its position in the xy plane of the device, within the oxide above the Si nanowire. The obtained k_{e} is shown in Fig.4a.

Results show a very fast decrease of the emission rate of the defect with the gate-defect distance, with values of k_{e} spanning from $k_{\mathrm{e}} = 10^{9}\,\mathrm{s}^{-1}$ when the defect is essentially in contact with the gate, to being completely frozen at large d. Note that the simulated spin qubit device contains several gates (white areas in the 2D map of Fig. 4a), so there are different spots within the device with maximal k_{e}. This can result in defects capturing and/or emitting at the same rate in different positions. The sharp exponential decay of k_{e} with d is highlighted in Fig. 4b. We can assign a characteristic length scale ℓ for this decay:

$$\ell = \frac{\hbar}{\sqrt{2 m_t V}}, \tag{4}$$

so that we can rewrite the dependence of k on d as

$$k(d) = k(d=0) \cdot \exp\left(-\frac{d}{\ell}\right). \tag{5}$$

We found a decay distance for the emission in Fig. 2b of $\ell = 0.19$ nm, in line with Ref. [12]. Note that, as mentioned above, all capture events experience the same V, so ℓ is the same for all k_{c} ($\ell = 0.15\,\mathrm{nm}$). For emissions, however, each defect experiences a different decay distance depending on its own ΔE. We report the distribution of ℓ for all emission processes in Fig. 4c. We indeed observe some scattering, with minimal values of $0.15\,\mathrm{nm}$, and maximal values slightly above $0.19\,\mathrm{nm}$. The decay remains nonetheless very sharp in all cases. Consequently, both capture and emission events are very unlikely to occur if the defect is located a few nanometers away from a gate.

Fig. 5 presents the shifts of the qubits coulomb peak ($\Delta\mu$) induced by the charge transfer of an individual defect placed in the hole spin qubit device shown in Fig. 1. We simulated

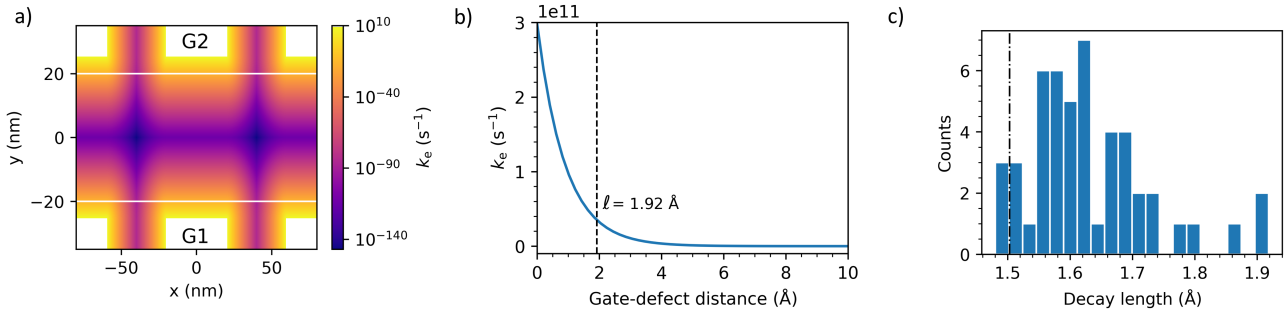

Fig. 4. a) Dependence of the charge emission rate of an individual defect with $\xi = 1.44 \cdot 10^{-1}\,\mathrm{eV}^{-1}$ (largest ξ_e in Fig. 2) on its position within the spin qubit device of Fig. 1. The defect is placed in the SiO_2 lying above the Si channel in the (xy) plane. The area within this plane that is covered by gates is highlighted in white, and the dashed ellipsoid illustrates the position of the qubit within the device. The temperature is set to 1 K. b) Decay of k_e as a function of the gate-defect distance. The data is a 1D cut at x=0 nm of the two-dimensional dependence for the HB defect in a). The horizontal dashed line highlights the characteristic decay distance ℓ for the emission process. c) Histogram of ℓ for the emission of the 46 studied HB defects. The horizontal dashed line highlights the $\ell = 0.15$ nm of all hole capture events.

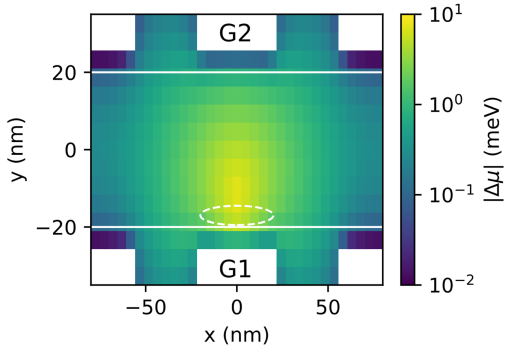

Fig. 5. Dependence of the chemical potential shift ($\Delta\mu$) induced by an individual defect on its position in the device of Fig. 1. The defect position is sampled in the same (xy) plane as in Fig. 4. The dashed ellipsoid illustrates the position of the qubit within the device.

a quantum dot (QD) by applying an attractive potential on gate G_1 ($V_{G_1} = -50\,\mathrm{mV}$, with $V_{G_2} = 140\,\mathrm{mV}$ and all other side gates grounded), and we sampled the position of the charged and neutral defect in the same xy plane of Fig. 4a. Results show that the shift of the coulomb peak can be as large as 10 meV when the defect is placed close to the QD. Nonetheless, given the sharp decay of k with d, these defects are unlikely to be active. The only defects that may remain active are those in close proximity to the metal gates. Interestingly, for these positions we observe smaller $\Delta\mu$, partly because of the defect being further from the qubit, but also because of the screening created by the metallic gates. Indeed, the defects that are more likely to be active are the least harmful for the qubits due to screening. $\Delta\mu$ for defects that are close to the metallic gates can still reach ~ 1 meV if the defect is located near G_1 (the closest gate to the qubit).

Fluctuations of the coulomb peaks of the order of a meV are significantly larger than typical charge noise amplitudes in spin qubit devices [5]. Combined with the slow dynamics of the HB defects, these results suggest that such charge transfer events may contribute to long-term device instabilities due to eventual charge emissions, but are unlikely to happen at frequencies relevant for qubit dephasing.

IV. Conclusions

We developed a simulation methodology for charge transfer processes which links atomistic defects to experimental spin qubit observables. Using HB defects in SiO_2 as a case study, we showed that charge transfer events are consistent with the slow, large-amplitude instabilities observed in spin qubit devices. Interestingly, their dynamics are too slow and their impact too strong to account for typical charge noise. This work highlights the potential of multi-scale simulations to uncover the atomistic origins of charge noise and related mechanisms that limit qubit performance and scalability.

V. Acknowledgment

This work was supported by the "France 2030" program (PEPR PRESQUILE-ANR-22-PETQ-0002) and was provided with computer and storage resources by GENCI at TGCC thanks to the grants 2024-AD010915504 and 2025-A0180616149 on the supercomputer Joliot-Curie's SKL and ROME partition.

References

[1] R. Maurand *et al.*, *Nat. Commun.*, vol. 7, no. 1, p. 13575, Nov. 2016.
[2] T. Bédécarrats *et al.*, in *2021 IEEE International Electron Devices Meeting (IEDM)*, 2021, pp. 1–4.
[3] B. Klemt *et al.*, *npj Quantum Information*, vol. 9, no. 1, p. 107, Oct 2023.
[4] B. Martinez *et al.*, *Phys. Rev. Appl.*, vol. 17, p. 024022, 2022.
[5] C. Spence *et al.*, *Phys. Rev. Appl.*, vol. 19, p. 044010, 2023.
[6] C. Wilhelmer *et al.*, *Microelectron. Reliab.*, vol. 139, p. 114801, 2022.
[7] J. Michl *et al.*, *IEEE Trans. Electron Devices*, vol. 68, no. 12, pp. 6365–6371, 2021.
[8] D. Waldhoer *et al.*, *Microelectron. Reliab.*, vol. 146, p. 115004, 2023.
[9] L. Shi *et al.*, *Phys. Rev. Lett.*, vol. 109, p. 245501, 2012.
[10] K. F. Freed *et al.*, *J. Chem. Phys.*, vol. 52, no. 12, pp. 6272–6291, 06 1970.
[11] L. Shi *et al.*, *Phys. Rev. B*, vol. 91, p. 205315, May 2015.
[12] Y.-Y. Liu *et al.*, *Phys. Rev. Appl.*, vol. 11, p. 044058, 2019.
[13] M. I. Vexler *et al.*, *Journal of Physics: Condensed Matter*, vol. 17, no. 50, p. 8057, dec 2005.
[14] Y. M. Niquet *et al.*, in *2020 IEEE International Electron Devices Meeting (IEDM)*, 2020, pp. 30.1.1–30.1.4.